Geoscience Data Journal

WILEY

Geoscience Data Journal | RMetS

DATA ARTICLE OPEN ACCESS

Intra-Island Variation in Wind Patterns on Sub-Antarctic Marion Island

J. Schoombie[1] | K. J. Craig[1] | K. A. Goddard[1] | D. W. Hedding[2] | W. Nel[3] | P. C. le Roux[4]

[1]Department of Mechanical and Aeronautical Engineering, University of Pretoria, Pretoria, South Africa | [2]Department of Geography, University of South Africa, Florida, South Africa | [3]Department of Chemical and Earth Sciences, University of Fort Hare, Dikeni, South Africa | [4]Department of Plant and Soil Science, University of Pretoria, Pretoria, South Africa

Correspondence: J. Schoombie (janine.versteegh@gmail.com)

Received: 21 March 2025 | **Revised:** 6 August 2025 | **Accepted:** 8 September 2025

Funding: This work was supported by South African National Research Foundation under the South African National Antarctic Programme (110726).

Keywords: aeolian processes | atmospheric modelling | computational fluid dynamics | high-resolution wind data | Marion Island | sub-Antarctic climate

ABSTRACT

Sub-Antarctic Marion Island provides a critical habitat for pelagic species, yet its terrestrial ecosystem faces increasing threats from climate change. Despite being situated in one of the windiest regions globally, the impact of changing wind patterns at the intra-island scale remains poorly understood. Existing datasets lack the spatial resolution necessary to capture fine-scale wind dynamics across the island. This study aimed to address this gap by presenting high-resolution wind speed and direction data to investigate the effects of wind on terrestrial systems. We present two complementary datasets: (1) wind measurements collected from 17 stations distributed across the island between May 2018 and March 2021, and (2) computational fluid dynamics (CFD) simulations providing wind vectors and associated properties at a 30 × 30 m resolution for heights up to 200 m above ground level. The data reveal significant differences in wind speed and direction across different geographical sectors of Marion Island. Notably, anemometers situated in the south recorded more frequent gale-force winds, while the western stations experienced calmer conditions. By using the observed wind direction frequencies, a weighted average vector plot was generated from the CFD simulations, providing an island-scale representation of spatial wind patterns across the island. These datasets offer valuable insights into variations in wind patterns, including upstream and downstream effects, and serve as a crucial resource for studying wind-driven processes affecting the landscape and ecosystem, such as seed dispersal.

Dataset Details

There are two datasets referred to in this paper. Both datasets and accompanying code are available on the South African Polar Research Infrastructure (SAPRI).

Titles and identifiers:

High-Resolution Wind Speed and Direction Data collected on Marion Island. DOI: https://doi.org/10.15493/SAPRI.23012025

Simulated Wind Vectors Across Marion Island for 16 Different Oncoming Wind Directions. DOI: http://doi.org/10.15493/SAPRI.07032025

Creator: Janine Schoombie

Dataset correspondence: janine.versteegh@gmail.com

Publisher: University of Pretoria

Publication year: 2025

Resource type: Dataset

1 | Introduction

Wind patterns in the Southern Ocean (SO) are dominated by a powerful and largely uninterrupted belt of westerly winds. These winds, known as the Southern Hemisphere Westerlies (SHW), play a crucial role in driving ocean currents (Lin et al. 2018; Swart and Fyfe 2012) and shaping the migration and foraging behaviour of seabirds (Clay et al. 2020; González-Solís et al. 2009; Richardson et al. 2018). Ekman-driven upwelling in the SO is vital for marine life, as it transports nutrient-rich waters to the surface (Anderson and Lucas 2009). Additionally, it plays a key role in global ocean circulation, shaping nutrient distribution and carbon cycling on a broader scale (Talley 2013).

Climate models predict that the SHW will intensify and shift southward in response to climate change (Perren et al. 2020; Swart and Fyfe 2012). These changes will significantly impact SO weather systems, ocean dynamics (Lin et al. 2018) and the unique habitats and species that have evolved across the SO (Constable et al. 2014).

On sub-Antarctic islands, wind is a critical ecological factor influencing both marine and terrestrial ecosystems (Toolsee and Lamont 2022). These islands serve as vital breeding grounds for pelagic animals that depend on land. Wind also shapes terrestrial ecology, influencing erosion, snow drift and accumulation, vegetation patterns, gene flow and nutrient cycling (Chau et al. 2019; Hedding et al. 2015; Momberg et al. 2021a; Smith and Mucina 2006). For example, strong winds can limit plant growth to sheltered areas, create wind-swept ridges and contribute to the dispersal of seeds and organic matter (Mazibuko et al. 2024; Momberg et al. 2021b).

Despite the importance of wind in these environments, intra-island wind variation remains poorly studied. Satellite datasets, such as the National Oceanic and Atmospheric Administration (see, e.g., National Center for Environmental Information, n.d.), or ERA5 reanalysis data (Copernicus Climate Change Service, Climate Data Store 2023), which offer minimum grid sizes of ca. 28×28 km (or ca. 0.25×0.25 degrees) that are too coarse to capture the fine-scale dynamics of islands like sub-Antarctic Marion Island (46°54′ S, 37°43′ E). At its widest, Marion Island is only 22 km, and the single weather station on the island, located on its eastern side in the lee of 1200 m-high interior peaks, cannot adequately represent island-scale wind patterns.

The goal of this study was to document intra-island wind data for Marion Island by (1) collecting wind measurements from multiple locations over multiple seasons and (2) developing a mechanistic computational fluid dynamics (CFD) model of wind flow to accurately simulate wind conditions across the entire island under different incoming wind conditions. The observed wind data, collected between 2018 and 2021, are valuable for quantifying fine-scale spatio-temporal variation in wind conditions and were used to validate the CFD model. The CFD output provides high-resolution wind vectors (30×30 m) for a range of broad-scale wind patterns (i.e., varying approaching offshore wind speeds and directions) and detailed wind patterns across the island's rugged and heterogeneous topography.

The datasets are particularly valuable because they provide unprecedented insights into intra-island wind flow patterns in one of the world's windiest regions. The data have already been used to investigate the influence of wind conditions on vegetation patterns (Mingione et al. 2025; Momberg et al. 2021a), fine-scale plant species distributions (Momberg et al. 2021b), wind dispersal of seeds (Mazibuko et al. 2024) and the associated gene flow patterns (Born et al. 2012) and nest-site choice by albatrosses (Momberg et al. 2023).

Potential applications of these datasets include examining the effects of wind on ecosystem functioning (e.g., spatial variation in primary productivity and decomposition rates), species physiology and morphology, plant-plant interactions and the impacts on pollination. The datasets will also provide insights into the dynamics of aeolian (wind-driven) sediment transport as well as landform development and modification across the island (see Hedding et al. 2015).

In this paper, we present the data collection methods, provide a comprehensive summary of the observed wind data and the CFD simulations, and discuss the recommended applications and limitations of the data. All measured data, except comparative data sourced from the South African Weather Service (SAWS), are made available on the South African Polar Research Infrastructure (SAPRI) Data Centre (Schoombie and le Roux 2025; Schoombie et al. 2025).

2 | Data Description and Developments

Wind data were obtained through two complementary approaches, described here as two datasets: (1) the installation of wind anemometers to measure wind speed and direction and (2) the use of numerical simulations. The measured data provided time-series insights into wind behaviour around the island and also enabled validation of the CFD model. Accordingly, the methods for collecting measured data are presented first, as they form the foundation for subsequent analyses. The CFD modelling approach is then discussed, with additional reference to the work of Goddard et al. (2022).

2.1 | Study Site

Marion Island is the larger of the two Prince Edward Islands (Figure 1) and has an area of ca. 293 km^2 (Rudolph et al. 2022). Meteorological measurements as well as regular research into the island's terrestrial ecology and geology date back to the 1940s (Chown and Froneman 2008). The wind direction measured at the research station on the east coast of the island has shown consistent westerly (i.e., blows from west to east, ca. 270°) and west-north-westerly winds (ca. 293°) between 1960 and 1980 (Rouault et al. 2005). The mean monthly wind direction for the period between 1980 and 2001 has shown an increased northerly component in the wind direction (Rouault et al. 2005). These changes have largely been attributed to the poleward shift in the SHW (le Roux 2008).

The island experiences gale-force winds ($> 15\,m \cdot s^{-1}$) for over 100 days per year, with an average wind speed of ca. $8\,m \cdot s^{-1}$

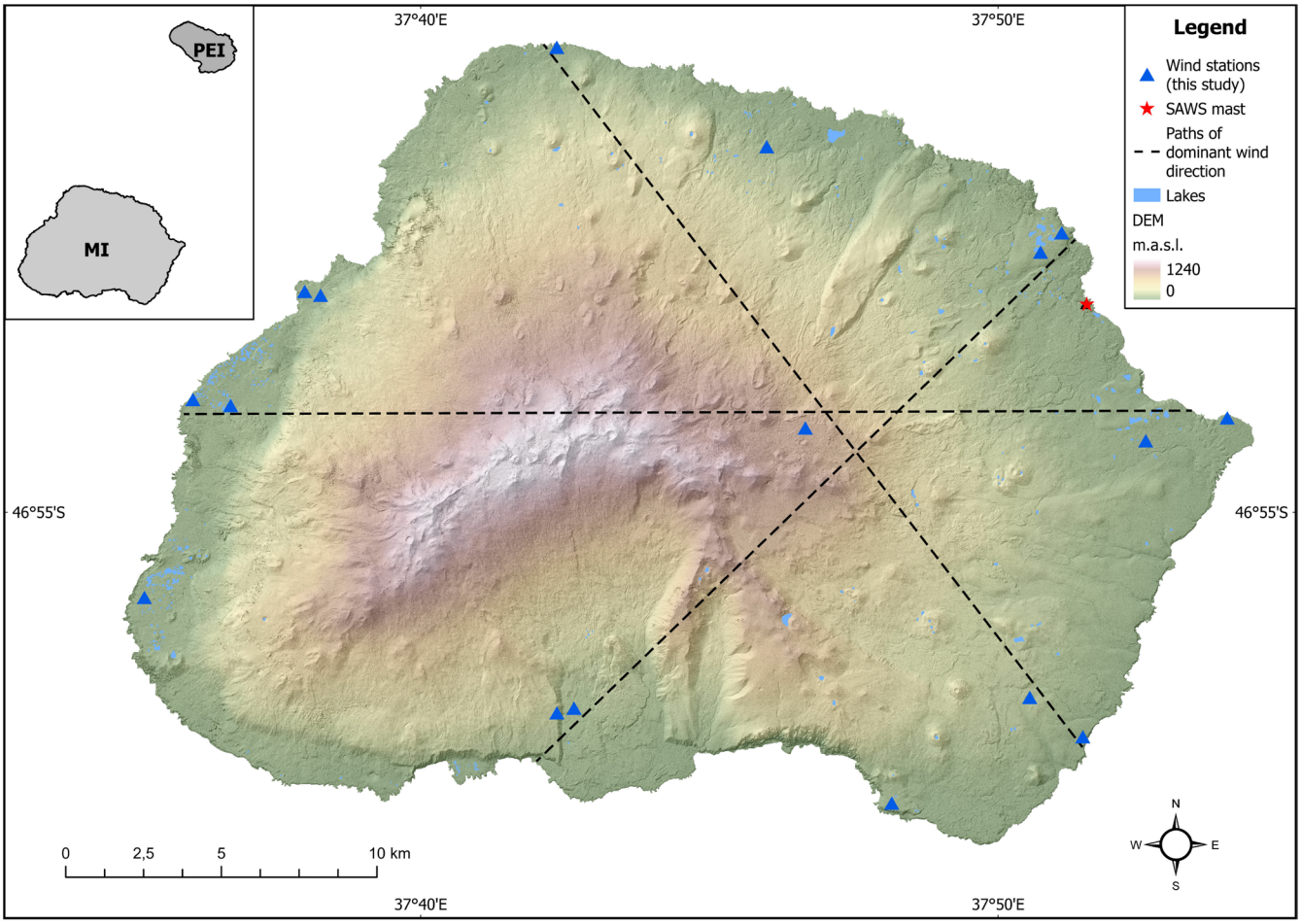

FIGURE 1 | Map of Marion Island with wind stations (triangles, see also Table 1) installed in 2018 and the South African Weather Service (SAWS) mast at the research base (star). The dashed black lines indicate the alignment with the expected dominant wind directions—southwesterly, westerly and northwesterly—which guided the placement of the stations. The insert (top left) shows Prince Edward Island to the northeast of Marion Island.

(Hedding et al. 2015). However, over the past 50 years, westerly winds have become less frequent, while northerly winds have increased in both frequency and strength (le Roux 2008). Considerable spatial variation in wind speed across the island has also been noted, but typically not quantified (le Roux 2008; Huntley 2016; although see, e.g., le Roux and McGeoch 2008a, 2008b).

Marion Island hosts a unique collection of plant and animal species, many of which exhibit adaptations to the windy conditions experienced on the island. For example, at mid- and high altitudes, the habitat is dominated by cushion plants (e.g., *Azorella selago*) and mosses, which typically display prostrate growth and streamlined surfaces, presumably as an adaptation to the strong winds (Combrinck et al. 2020; Smith and Mucina 2006). Several of the region's insect species are functionally flightless (e.g., *Pringleophaga marioni*, see Chown and Convey 2016), while seabirds like albatrosses and petrels are adapted to take advantage of the strong winds. However, wind can also impact their foraging strategies (Clay et al. 2020; Thorne et al. 2023) and their ability to reach breeding sites on land (Schoombie et al. 2023). Many of these species appear to be highly sensitive to changes in climatic conditions (e.g., le Roux and McGeoch 2008a, 2008b; Weimerskirch et al. 2012; Chown et al. 2013), and further changes in wind dynamics on and around the sub-Antarctic islands could potentially substantially impact these ecosystems (e.g., via changes in habitat structure, foraging ability and reproductive success). Hedding et al. (2015) quantify annual (horizontal) aeolian sediment flux at 0.36–3.85 kg $cm^{-2}.y^{-1}$ at 0.05 m above the ground for a selected site on Marion Island. These rates are expected to increase if the island continues to experience climatic amelioration through higher air temperatures (Nel et al. 2023) and lower precipitation totals leading to vegetation die-back and drying out mire lakes and peats (Hedding and Greve 2018).

2.2 | Measured Wind Data

2.2.1 | Equipment Setup

Between April 2018 and May 2021 (ca. 35 months), 34 Gill WindSonic two-dimensional (2D) sonic anemometers were installed in 17 different locations around Marion Island (Figure 1, see also Table 1). At each location, a wind station consisting of two anemometers, one at 0.5 m and one at 1 m above ground level (a.g.l.), was erected (Figure 2). The maximum height of 1 m was dictated by environmental concerns: a taller mast would increase the risk of bird collisions and would require permanent fixtures (which is not allowed

TABLE 1 | Wind station geographic coordinates and altitude.

Station number	Site name[a]	Latitude [°]	Longitude [°]	Altitude [m.a.s.l]	Date installed	Date removed
1	Swartkops	−46.9333	37.58689	29.5	2018/04/23	NA
2	Kampkoppie Inland	−46.8954	37.61177	43.2	2018/04/22	2020/02/09
3	Kampkoppie Coastal	−46.8942	37.60090	25.3	2018/04/22	NA
4	Mixed Pickle Coastal	−46.8729	37.63315	23.9	2018/04/21	2019/08/03
5	Mixed Pickle Inland	−46.8737	37.63773	61.4	2018/04/21	2020/02/08
6	Cape Davis	−46.8247	37.70592	88.9	2018/05/12	NA
7	Repettos	−46.8444	37.76653	94.2	2018/04/20	2020/02/07
8	Katedraal	−46.8999	37.77768	739.1	2018/05/09	NA
9	Skua Ridge Inland	−46.9560	37.70595	279.8	2018/04/16	NA
10	Skua Ridge Coastal	−46.8614	37.85169	61.4	2018/04/26	NA
11	East Cape Inland	−46.9024	37.87594	39.5	2018/04/27	NA
12	East Cape Coastal	−46.8979	37.89948	18.3	2018/04/17	2020/02/25
13	Kildalkey Inland	−46.9530	37.84247	136.8	2018/04/30	2020/02/15
14	Kildalkey Coastal	−46.9607	37.85777	44.1	2018/04/29	NA
15	Puisie	−46.9738	37.80262	78.6	2018/04/29	NA
16	Grey Headed Ridge	−46.8652	37.84558	69.2	2018/06/02	NA
17	Santa Rosa Valley	−46.9551	37.71091	112.6	2018/06/02	2020/03/19

Note: See Figure 1 for a map of these locations.
[a]Names and a detailed description of Marion Island are available from (Rudolph et al. 2022).

FIGURE 2 | Wind station installed on the western side of Marion Island. The anemometers are at heights of 0.5 and 1 m above the ground surface. The blue sleeve across the horizontal arm of the 0.5 m anemometer was installed to stop mice from accessing the 0.5 m anemometer.

under the current management of the island, Department of Environmental Affairs 2010). Given the low stature of the vegetation, data at or below 1 m a.g.l. are most ecologically relevant in this terrestrial ecosystem.

The locations of eight wind stations were chosen based on the expected wind direction (owing to data from the island's weather station and general circulation patterns; Figure 1): two stations on the windward side and two on the leeward side to align with winds blowing from the three expected dominant directions (southwest, west and northwest). Most stations were installed on flat, open coastal terrain to ensure locally uninterrupted wind flow (see also Section 2.5) and allow reliable access for maintenance and data retrieval. Five stations were also placed at the locational extremes, one each for north, east, south, west and central at high altitude. Four stations were placed around landforms of specific interest (e.g., station 9, see Schoombie et al. 2023) or to fill geographic gaps (e.g., station 7). While every effort was made to install the wind stations in line with the predetermined wind directions (see dashed lines in Figure 1), the final installation locations were dictated by local topography and the proximity to bird colonies.

One concern about the wind station design was the potential for the mast (for the 1 m anemometer) to interfere with the 0.5 m anemometer. Given the rarity of easterly winds (based on the wind data available at the time of installation), the pole supporting the 0.5 m anemometer was oriented towards the west (i.e., minimising the potential for winds blowing around the mast to affect readings of the 0.5 m anemometer). Additionally, guy wires were anchored as low as possible to limit any potential influence on the anemometer measurements.

The data from each anemometer were collected at 0.2 Hz and stored as 10-min, hourly and daily averages with standard deviations, via a CR300 Campbell Scientific data logger n.d. These data outputs are referred to as 'data tables' throughout this paper (i.e., the wind measurement dataset consists of three data tables, one for each averaging period). Each station was powered by a 22 V solar panel connected to a 12 V DC battery. Wind direction always indicates the direction from where the wind is blowing. For example, a northwesterly wind (NW) blows from the northwest to the southeast.

2.2.2 | Data Cleaning

To evaluate possible outliers, we defined a speed height ratio (R_u), that is the ratio of speed measured at 0.5 m and 1 m a.g.l.:

$$R_u = \frac{U\_mean\_0.5m}{U\_mean\_1m} \quad (1)$$

Because of the nature of the atmospheric boundary layer (ABL), we expect U_mean_0.5 m to be less than U_mean_1m ($R_u < 1$). Some U_mean_0.5 m values were well above U_mean_1m ($R_u >> 1$), but within the anemometers' measurement range (i.e., > 60 m/s; (Gill Instruments Limited 2017)). This raises uncertainty about whether the values are due to a programming error or reflect real conditions. To determine a reasonable threshold of acceptable speed height ratio (R_u), the number of measurements below a given speed ratio threshold was plotted using the 10-min data from all 17 locations. To be conservative, all measurements where $R_u > 2$ – well above the 98th percentile – were removed (< 0.03% for all three data tables).

All 0.5 m anemometers showed signs of mouse damage, and some outliers may be linked to animal activity. Outliers were most common during months with heavy ice and snowfall, particularly at higher-elevation Stations 8 and 9 (740 m and 280 m a.s.l.). Snow and ice buildup (riming) likely interfered with measurements (Gill Instruments Limited 2017). Data points with outlier R_u values were removed, affecting less than 0.04% of all 10-min, hourly and daily records.

Two wind stations recorded U_max_0.5 m = 1000 m · s^{-1}, which is beyond the capability of the anemometers. All 1 m measurements indicated errors (i.e., giving NAN values) when 0.5 m anemometers' maxima were given as 1000 and since the cause of this error could not be ascertained, these data points were removed from the dataset (< 0.004% for hourly and 10-min data, and < 0.14% for daily data).

All data points where both the 1 and 0.5 m anemometers recorded NAN values were removed from the dataset (< 0.6% for all three data tables). For the high-altitude station (Station 8), NAN values were present when the wind speed exceeded the maximum speed measurement capacity of the anemometers and during periods of snow cover (anemometers were covered in ice for weeks at a time during winter). In the final dataset, the recorded NAN values indicate where one of the anemometers was removed but the other remained in place (e.g., if one of the anemometers was damaged or removed).

An unidentified programming error has resulted in the value '−8.191' being recorded in place of actual measurements ($n = 14$). Since the root cause of this error remains unknown, each affected row was removed, constituting < 0.01%, 0.1%, and 2.1% of the 10-min, hourly and daily data tables, respectively. The higher proportion of errors in the daily data table reflects the fixed number of erroneous '−8.191' entries, which become proportionally larger as the sampling interval decreases. In total, all NAN and erroneous values removed from the dataset amount to 0.6% of the hourly and 10-min datasets and 2.4% for the daily dataset (see details in Table 2).

2.3 | Simulated Wind Data

2.3.1 | Simulation Domain

In the CFD simulations, a volume of air was defined around a 1 × 1 m digital elevation model (DEM) of Marion and Prince Edward islands (Rudolph et al. 2022). The simulations were conducted using ANSYS Fluent 2019R3 software (ANSYS Inc. 2025). Given the subsonic and incompressible nature of the airflow around these islands, atmospheric interactions between the two land masses were anticipated, especially for northerly to easterly wind directions, requiring both islands to be modelled together within the same computational domain.

TABLE 2 | Percentage of data excluded due to outliers, NAN values and erroneous measurements.

Station number	Station name as recorded in the data files	Data removed during cleaning (%)		
		10-min data	Hourly data	Daily data
1	Marion_Wind_ST1	0.01	0.08	2.10
2	Marion_Wind_ST2	0.09	0.17	2.52
3	Marion_Wind_ST3	0.04	0.11	2.78
4	Marion_Wind_ST4	0.01	0.08	2.09
5	Marion_Wind_ST5	0.25	0.29	1.97
6	Marion_Wind_ST6	0.1	0.18	2.06
7	Marion_Wind_ST7	0.05	0.09	2.05
8	Marion_Wind_ST8	8.01	6.61	4.09
9	Marion_Wind_ST9	0.18	0.23	2.34
10	Marion_Wind_ST10	0.03	0.08	2.08
11	Marion_Wind_ST11	0.03	0.09	2.01
12	Marion_Wind_ST12	0.01	0.08	2.31
13	Marion_Wind_ST13	0.06	0.10	2.24
14	Marion_Wind_ST14	0.02	0.09	1.77
15	Marion_Wind_ST15	0.02	0.07	2.04
16	Marion_Wind_ST16	0.03	0.09	2.28
17	Marion_Wind_ST17	0.34	0.10	3.63

The topographical data for Marion and Prince Edward Islands were provided in GeoTIFF format, a raster data file type commonly used in geosciences but incompatible with ANSYS Fluent for geometry definition. To address this, a gradient-based resampling algorithm was applied to the GeoTIFF files, reducing the number of stored pixels while preserving the essential shape and topography of the islands. The resampled data were then converted into stereolithography format, making them compatible with ANSYS Fluent and allowing for efficient geometry representation with considerably fewer points.

The fluid volume (i.e., the simulated volume of air surrounding the island with upstream and downstream regions of the surrounding sea surface included) was discretised into an unstructured grid comprising ca. 140 million polyhedral cells, with a grid spacing of 30 × 30 m at the island surface. Prism layers were used at ground level to resolve the expected high gradients in velocity magnitude. A mesh dependence study confirmed that these specifications provided mesh-independent results (see Goddard et al. 2022).

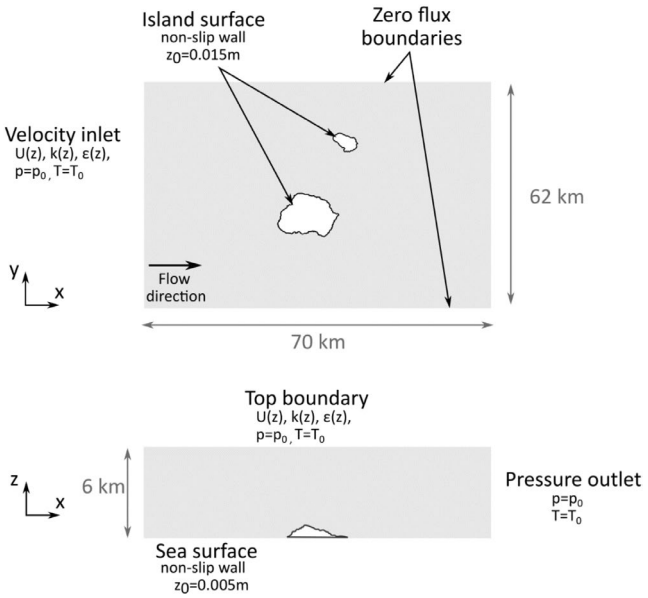

FIGURE 3 | Schematic presentation of the fluid domain size and boundary conditions for numerical simulations (not to scale).

2.3.2 | Boundary Conditions

The wind speed and direction – along with other environmental conditions – are specified at the inlet boundaries of the fluid volume (see Figure 3), and the physics of the airflow (including pressure and velocity components) is iteratively calculated across the grid using the Reynolds-averaged Navier-Stokes equations. Unlike transient or predictive atmospheric models, which simulate changes in flow over time, these simulations are steady-state, representing the flow at a single point in time without forecasting temporal evolution. In this study, we conducted steady-state simulations for 16 cardinal wind directions at a single moderate wind speed, which was determined based on the measured wind speeds. As the focus of the CFD simulations was

on capturing low-altitude wind patterns, a neutrally stable atmosphere was assumed, implying that the energy conservation equation was not solved.

For each direction, the inlet velocity (Figure 3) was configured to reflect the ABL profile using Equation (2). These profiles were applied on the flat sea surface at $z=0$, hence not requiring terrain-following coordinates (Hargreaves et al. 2006).

$$U(z) = \frac{u_*}{\kappa} \ln\left(\frac{z + z_0}{z_0}\right) \tag{2}$$

where $U(z)$ is the horizontal speed as a function of z, which is the height above sea level, u_* is the friction velocity, k is the von Kármán constant (0.41) and z_0 is the surface roughness. The friction velocity u_* was calculated to be $0.735\,\mathrm{m}\cdot\mathrm{s}^{-1}$ from the measured wind data using the speed recorded by the 1 and 0.5 m anemometers (Equation 3). Standard sea-level properties were used for the density and dynamic viscosity.

$$u_* = \frac{\kappa}{2}\left(\frac{|\mathrm{U\_mean\_1m}|}{\ln\left(\frac{1}{z_0}\right)} + \frac{|\mathrm{U\_mean\_0.5m}|}{\ln\left(\frac{0.5}{z_0}\right)}\right) \tag{3}$$

where U_mean_1m and U_mean_0.5 m are the speeds measured at 1 and 0.5 m, respectively.

The turbulence in the simulations was approximated with the k-ε turbulence closure scheme (Launder and Spalding 1974), a turbulence model often used as the basis for atmospheric flows, with modifications to the model constants as discussed below. The vertical profiles for the turbulent kinetic energy (k) and the dissipation rate (ε) were also specified at the velocity inlet using Equations (4) and (5).

$$k(z) = \frac{u_*^2}{\sqrt{C_\mu}}\left(1 - \frac{z}{z_h}\right)^2 \tag{4}$$

$$\varepsilon(z) = \frac{u_*^3}{\kappa(z + z_0)} \tag{5}$$

$C_\mu = 0.03$ is a k-ε model constant (based on modifications from Cabezón et al. 2011) and z_h is the estimated boundary layer depth, calculated for neutral stratification as

$$z_h = 0.2\frac{u_*}{|f_c|} \tag{6}$$

Here, $f_c = -1.06\times10^{-4}\,\mathrm{s}^{-1}$ is a Coriolis force parameter, based on the earth's rotation and latitude (Crasto 2007).

To maintain a horizontally homogeneous ABL profile across the simulation volume, the top boundary was specified as a velocity inlet, with $U(z)$, $k(z)$ and $\varepsilon(z)$ calculated using Equations (2) and (4–6) (Figure 3). The surfaces of both islands were assigned a no-slip boundary condition, implying shear forces were calculated as a result. The boundary layer was resolved by the CFD algorithm with a land surface roughness (z_0) of 0.015 m (representative of rough pasture, as per Manwell et al. 2009). A flat no-slip surface, with $z_0 = 0.0005$ m, was used to model the sea surface, approximating a wind-blown ocean surface (see more detail in Goddard et al. 2022). A minimum first-cell height of 0.2 m was chosen throughout the domain to ensure that the centroid of the first cell is above the equivalent sand grain roughness (a parameter related to the surface roughness (Goddard et al. 2022; see also Goddard 2021)).

Symmetry (i.e., reflection) boundary conditions were applied at the side boundaries of the flow domain. This approach effectively mirrors the system along these faces. An outflow boundary condition was specified at the outlet of the domain, enforcing no gradients in quantities at this face, located sufficiently far downstream of the islands (Figure 3) based on a domain-dependence study (Goddard 2021; Goddard et al. 2022). Sixteen simulations were carried out for different freestreams (i.e., undisturbed flow approaching the island) wind direction inputs (22.5° angular bins) at the inlet and top boundaries: north (N), north-northeast (NNE), northeast (NE), east-northeast (ENE), east (E), east-southeast (ESE), southeast (SE), south-southeast (SSE), south (S), south-southwest (SSW), southwest (SW), west-southwest (WSW), west (W), west-northwest (WNW), northwest (NW) and north-northwest (NNW).

Different wind directions were simulated by rotating the far-field boundaries around a near-field cylindrical volume surrounding the island surfaces (light-blue circles in Figure 4). The stationary near-field mesh ensures a consistent mesh for all simulations and simplifies the inlet definitions for different wind directions.

2.4 | Technical Validation

2.4.1 | Measured Data

Technical validation of the dataset was ensured through regular maintenance and calibration of the equipment. Anemometer directionality was verified in a controlled environment using the 2-m wind tunnel at the Council for Scientific and Industrial Research. This process confirmed the accurate interpretation of wind directions as programmed into the data logger by the supplier, Campbell Scientific Africa. A detailed maintenance schedule was followed, with checks conducted monthly during the first 2 years of installation in the field, and every 2 months in subsequent years. These checks included downloading data, verifying the orientation of the anemometers, assessing battery state, and comparing real-time wind speed and direction measurements with handheld anemometers during data retrieval.

2.4.2 | Simulated Fine-Scale Data

A thorough and detailed validation was carried out for the CFD simulations using a subsample of the measured data

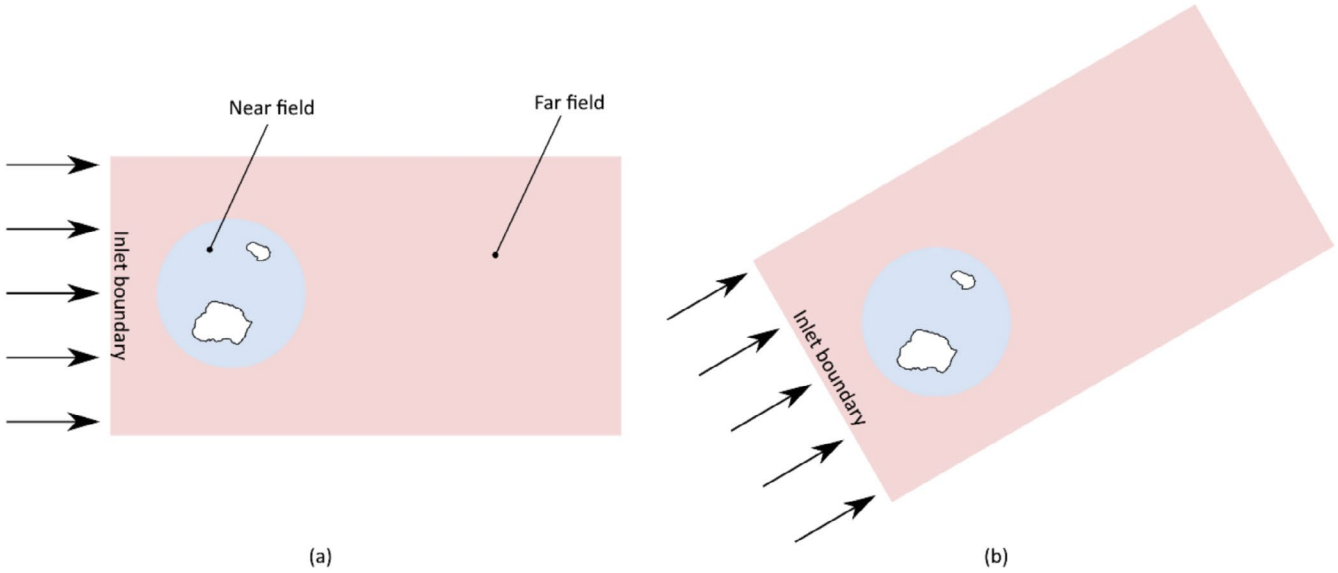

FIGURE 4 | Illustration of the fluid domain for (a) westerly and (b) southwesterly wind inlet conditions.

(Goddard 2021; Goddard et al. 2022). However, the sample size of measured wind data was sufficient only for the dominant wind directions, NW, SW and W. Consequently, CFD results were validated for these specific freestream wind directions by comparing them to subsets of the observed wind data corresponding to each direction. While detailed information on this process and statistical metrics is available in Goddard (2021) and Goddard et al. (2022), some key points are reiterated here for clarity.

The simulated wind speeds showed good agreement with measured data for the W and SW wind directions (prediction accuracy of 97% and 94%, respectively) while the correlation was less accurate for the NW direction (prediction accuracy of 82%). The simulated wind directions showed varying accuracy compared to measured data, with prediction rates of 85% for W, 100% for SW and only 64% for NW freestream conditions. The primary source of error was the approach used to model the Coriolis effect, which resulted in an exaggerated turning of the flow, impacting the directional accuracy.

Discrepancies between the measured and simulated flow were most evident in the lee of terrain features, where more turbulent air flow patterns are expected to occur. As a result, greater variability can be expected in the measured wind conditions in the lee of landscape features, and larger discrepancies between observed and simulated wind characteristics are likely due to this natural variation rather than flaws in the CFD approach (which simplifies the flow to a steady-state condition with an estimate of turbulent intensity based on steady-state turbulent kinetic energy and its dissipation).

However, this approach still provided an overall strong prediction. Despite these limitations, the model performed well, achieving accurate predictions in 91.2% of cases and a mean directional error of 8.23%, corresponding to 14.8°. The fine-scale data produced by this model, which were previously unavailable, have since been used effectively in various studies (examples and references).

2.5 | Preliminary Observations

The measured wind speeds and directions are 2D, capturing only the horizontal plane without any vertical component. This could result in slightly lower speed measurements compared to a full 3D vector magnitude if there is a significant vertical component. We minimised this potential effect by positioning stations in flat areas, so any discrepancy is expected to be minor, but users of these data should keep this limitation in mind.

For the statistical analyses, the daily means were used in analyses and visualisations to avoid issues of temporal autocorrelation, unless stated otherwise. To streamline the analysis and ensure clarity in the figures presented, we defined five geographical sectors as reference areas, each with one representative station per sector, informed by the wind rose diagrams in Figure 5.

In the Western sector (Figure 5), Stations 2 and 3, and Stations 4 and 5 are paired geographically, separated by ca. 840 and 360 m, respectively. Stations 2 and 3 exhibited similar wind direction and speed patterns, as did the data from Stations 4 and 5, which were also closely aligned with those of Stations 2 and 3. However, Station 1 displayed visually different behaviour compared to the others. Station 3 was selected as the representative for this sector because it is located furthest from the escarpment, a feature likely to have a substantial influence at this elevation.

For the Northern sector, Stations 6 and 7 showed differing patterns (Figure 5), but the coastal location of Station 6 made it less likely to be affected by topography and thus more likely to represent wind conditions in the northern sector of the island.

In the Eastern sector, Stations 16 and 10 closely matched the SAWS data in terms of directional modes, while Stations 11 and 12 showed similar patterns to each other. Station 11 was chosen as the representative for this sector due to its location

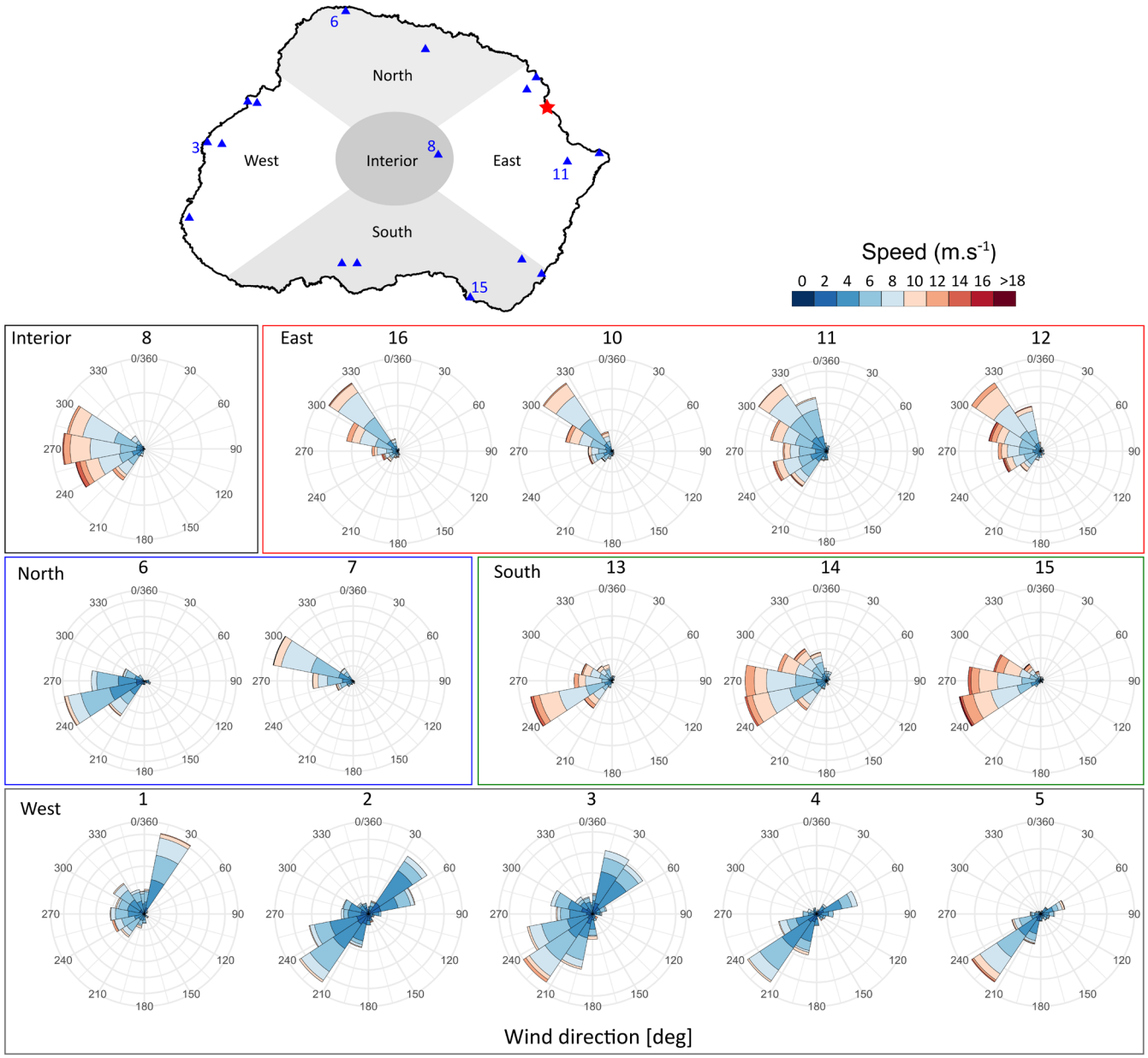

FIGURE 5 | Wind roses for all stations within the five geographical sectors around Marion Island. To ensure a consistent representation of data across all stations, the data are limited to a common timeframe, from the latest start date (2018-05-22; see also Table 1) to the earliest end date (2020-02-08). The station numbers are given above each wind rose.

on level terrain, far from landforms that could strongly affect wind patterns.

For the Southern sector, Stations 13, 14, and 15 all presented similar directional modes, with Station 15 selected as the representative station as it is situated in the flattest area near the coast, with minimal expected influence from the surrounding topography. Stations 9 and 17 are paired geographically near a large ridge (Grey-headed Albatross Ridge; i.e., a feature of interest; Schoombie et al. 2023) and likely do not provide a fair representation of wind in the southern sector of the island.

Lastly, the Interior sector was represented solely by Station 8, situated at approximately 740 m above sea level, and is the only station located in the island's central highland.

Stations 3, 6, 11 and 15 provided complete datasets spanning the entire study period, making them the most reliable choices for representing their respective sectors. In contrast, some of the other stations encountered damage or technical issues, resulting in incomplete data that limited their suitability for direct comparisons.

2.5.1 | Correlation Between 0.5 m and 1 m Measurements

The data from the 1 m and 0.5 m anemometers showed a strong correlation with respect to wind direction (279.6° ± 1.0° and 273.0° ± 1.0°, respectively; Figure 6). As anticipated, the mean wind speed from the 0.5 m anemometer (5.4 ± 2.3 m · s^{-1}) was noticeably lower than the 1 m anemometer (6.4 ± 2.6 m · s^{-1};

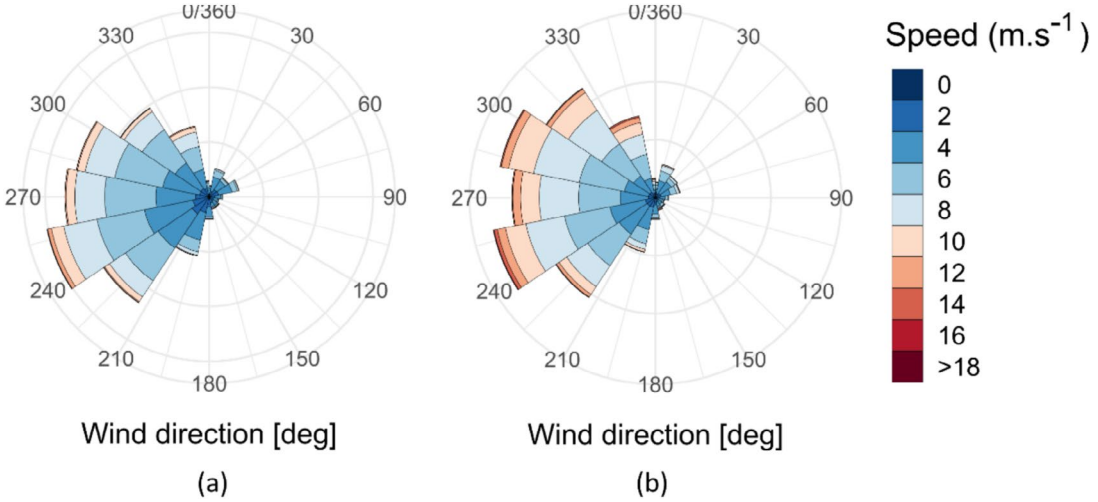

FIGURE 6 | Wind roses for the (a) 0.5 m and (b) 1 m data collected for all locations between 2015-05-22 and 2021-06-01 (~35 months). The height of each bar indicates the relative frequency of winds from a given direction, while the shading indicates the frequency of different wind speeds for each wind direction.

Figure 6). While a 0.5 m difference in height above the ground surface level may not be informative in all contexts, it is valuable for research conducted near the ground surface (e.g., botanical, entomological and geomorphological contexts on this island where vegetation height rarely exceeds 10–40 cm).

2.5.2 | Intra-Island Comparison

To illustrate the limitations of measuring wind at a single location on the lee side of Marion Island, data from the SAWS were incorporated into the analysis for demonstration purposes, although they were not formally included in the dataset.

The wind roses reveal distinct variations in dominant wind direction across different sectors of Marion Island (Figure 7, see also Figure 5), with some sectors exhibiting multiple directional modes (Table 3). The SAWS mast, positioned at 10 m a.g.l., predominantly records winds from the NW. Similarly, the eastern station in this study, located c. 3 km south of the SAWS mast and measuring at 1 m a.g.l., also shows a dominant NW mode (Table 3), although its directional distribution is more dispersed (Figure 7).

For the northern and southern sectors, the dominant wind directions are more WSW, with the southern sector experiencing higher average wind speeds (Table 3). On the western side of the island, however, the observed wind modes – NE and SW – deviate significantly from the other sectors. The NE mode is particularly unexpected, as the prevailing wind is anticipated to be predominantly W to NW, given the sector's exposure to incoming winds. This suggests that winds at lower altitudes in this sector are frequently from the NE, likely influenced by local topographic influences such as the western escarpment (see DEM in Figure 1). The escarpment follows a roughly NNE-SSW orientation. At the lower altitudes where measurements were taken, it appears that incoming W or NW winds may be deflected and channelled along the escarpment, resulting in stations recording a NE wind direction instead of the original NW or W flow. However, further investigation is needed to confirm this, ideally with offshore wind measurements.

In the interior, wind speeds are notably higher. The dominant directions in the interior resemble those measured by the eastern wind station, but the distribution of directions is more varied, and the mean wind direction is distinctly westerly. These results highlight that wind conditions measured at the location and height of the SAWS anemometers may not accurately represent near-ground conditions relevant to biotic and abiotic systems, which also vary significantly across the island. The unique wind direction modes observed on the western side of the island, in particular, warrant further investigation to better understand the influence of terrain on wind patterns.

2.5.3 | Frequency of Calm Versus Windy Days

There is considerable variation in the frequency of calm and gale force wind days (i.e., wind extremes) across the island. Here, we have defined calm conditions as the lower 2nd percentile of measured wind (i.e., $< 1.9\,\mathrm{m \cdot s^{-1}}$, equivalent to 'light air' on the Beaufort Scale; World Meteorological Organization 2008), and gale conditions are the 98th percentile (i.e., $> 12.1\,\mathrm{m \cdot s^{-1}}$, which is equivalent to gale-force winds according to the Beaufort Scale). The southern sector experiences considerably more days (80 days; Figure 8) with gale-force winds compared to the other coastal sectors (< 20 days). The interior was expected to have many more gale-force winds as it is at a high altitude, but these data are likely skewed because there were many more NAN measurements that we can reliably attribute to wind speeds above the measurement capacity of the anemometers. This limited the assessment of wind regimes in the mountainous interior of Marion Island. Nevertheless, within the context of 'calm' and 'gale' conditions, these observations are particularly significant for the geomorphology and terrestrial ecology of the island because gale force conditions will influence aeolian (wind-driven) sediment flux as well as landform development and modification (see Hedding et al. 2015) whereas calm conditions will limit seed dispersal (see Mazibuko et al. 2024).

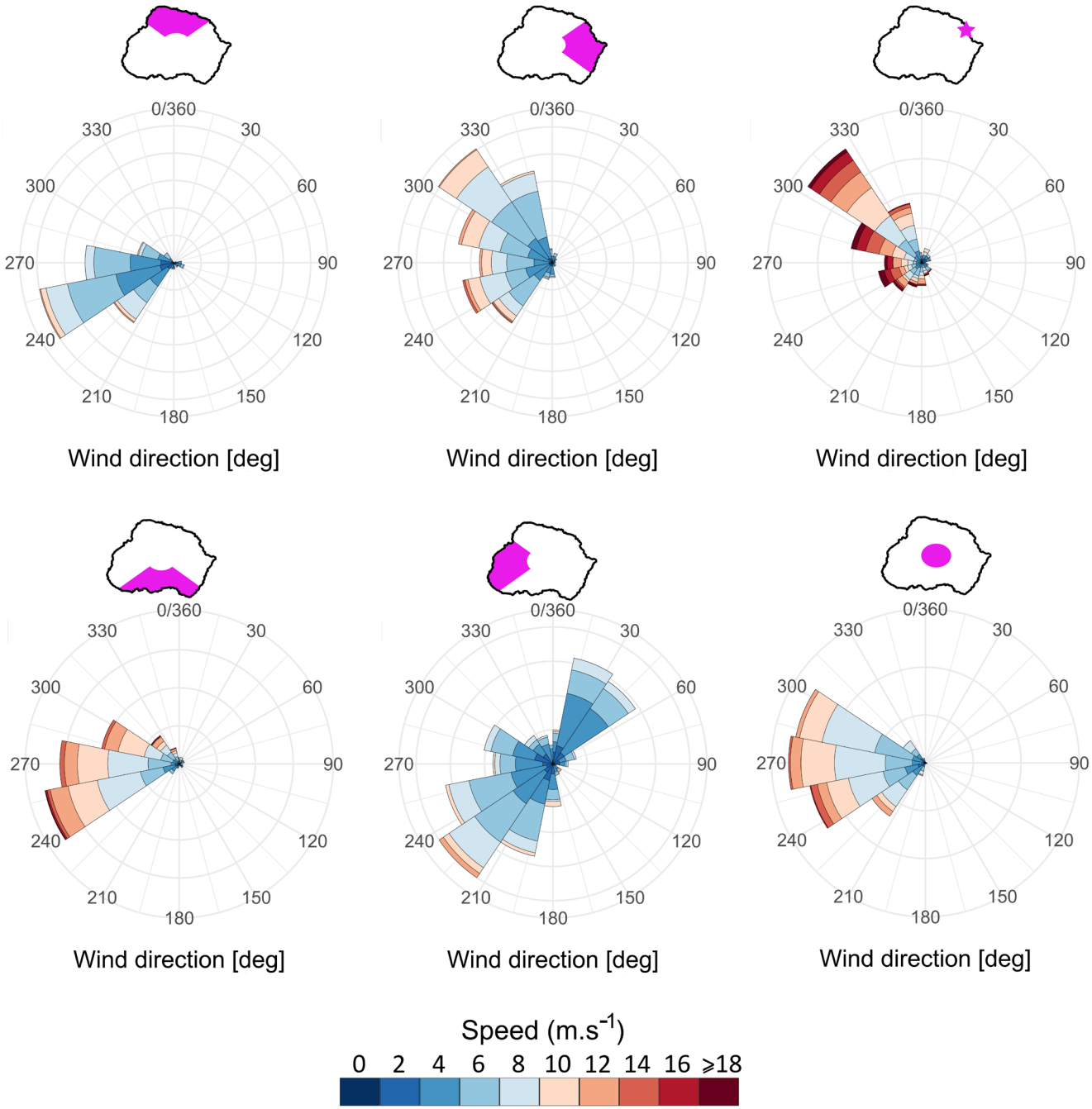

FIGURE 7 | Wind roses for each representative geographical sectors at 1 m a.g.l. alongside the South African Weather Service (SAWS) data at 10 m a.g.l. Sectors are illustrated above each corresponding wind rose and the SAWS mast location is marked with a star. See Table 3 for detailed statistics. The SAWS measurements, originally recorded as 5-min averages for wind speed and direction, were subsampled to daily values at noon to ensure consistency.

2.5.4 | Steady-State Fine-Scale Wind Vectors (CFD)

Sixteen simulations with wind directions in 22.5° increments (or bins) were simulated, with a constant speed input based on the ABL profile. In this dataset, the vectors can be plotted over the surface of the island at a constant height above ground.

The 16 CFD simulations (illustrating input wind) represent steady-state freestream wind conditions for each of the 16 cardinal directions. To estimate fine-scale wind patterns over time, a weighted average was calculated (Figure 9), using the frequency of each wind direction bin based on wind direction measured from the 5 geographical sectors. As expected, the averaged vectors are closely related to the vectors from the simulations with a strong westerly component as the inlet condition. We consider this to provide a representative summary of conditions.

The vectors reveal typical flow patterns, including accelerated flow over peaks and recirculation behind bluff landforms (Figure 10). At this scale, we can examine specific landforms under different freestream conditions. For example, in the

TABLE 3 | Summary of data collected between 22 May 2018 and 31 May 2021 (ca. 35 months) for the five representative stations, each corresponding to one of the five geographical sectors on Marion Island, at a height of 1 m above ground level.

Representative sector	Station number	Wind direction dominant mode(s)	Mean ± SD speed at 1 m a.g.l. ($m \cdot s^{-1}$)	Maximum wind speed at 1 m a.g.l. ($m \cdot s^{-1}$)
North	6	WSW	5.5 ± 2.7	35.0
East	11	NW, SW	6.3 ± 2.2	34.8
South	15	WSW	8.0 ± 2.9	40.3
West	1	NE, SW	5.0 ± 2.0	33.1
Interior	8	W (WNW to WSW)	7.4 ± 2.5[a]	59.7[a]
East	SAWS mast	NW	9.3 ± 4.4 (10 m a.g.l.)	34.5

Note: These data are visualised in Figure 7.
[a]Some gaps in data when speeds are > 60 $m \cdot s^{-1}$, i.e., greater than the capabilities of the anemometer, so this is possibly an underestimate.

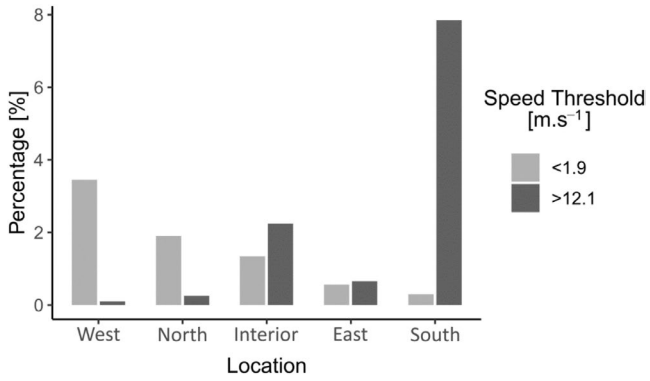

FIGURE 8 | Frequency of calm (< 1.9 $m \cdot s^{-1}$) and strong (> 12.1 $m \cdot s^{-1}$) daily wind speed averages measured at 1 m a.g.l. in the five representative geographical sectors over the study period.

western coastal area of the island, westerly winds shift SW as they approach the escarpment at 1 m a.g.l. (Figure 11). Similarly, when winds approach from the N or NW, they turn NE near the escarpment at 1 m a.g.l. (Figure 11). This likely explains why the western stations record both southwest and northeast directional modes. The wind vectors at 1 m a.g.l. for the whole island for eight of the 16 simulated wind directions are illustrated in Figures S1–S8.

3 | Available Data Records

Wind data from this study are stored in SAPRI Data Centre (https://www.sapri.ac.za/data-products-society/data/), which is a public access repository, hosted by the South African Environmental Observation Network.

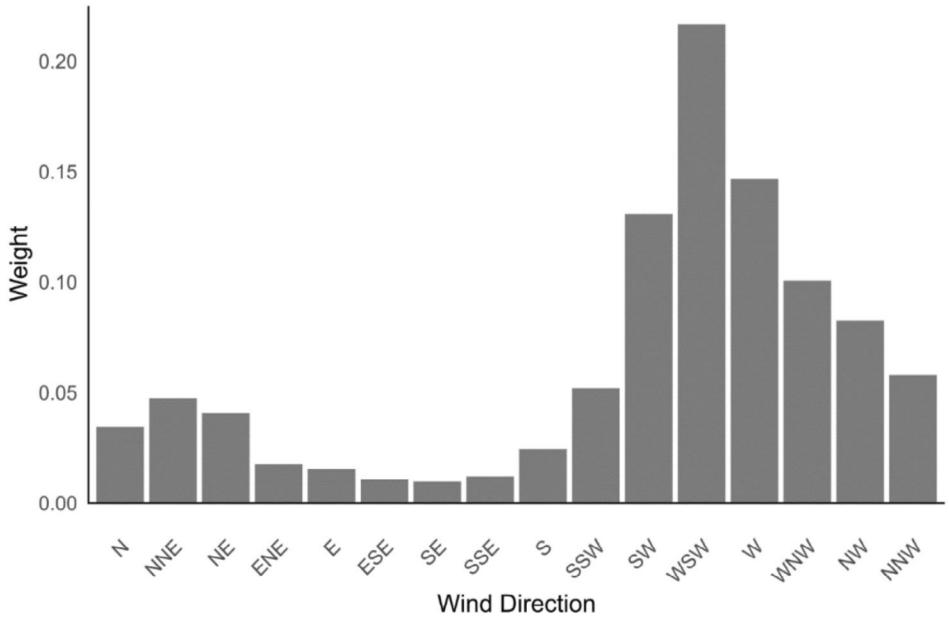

FIGURE 9 | Weights calculated for 16 cardinal wind directions as measured in the five geographical sectors on Marion Island during the study period.

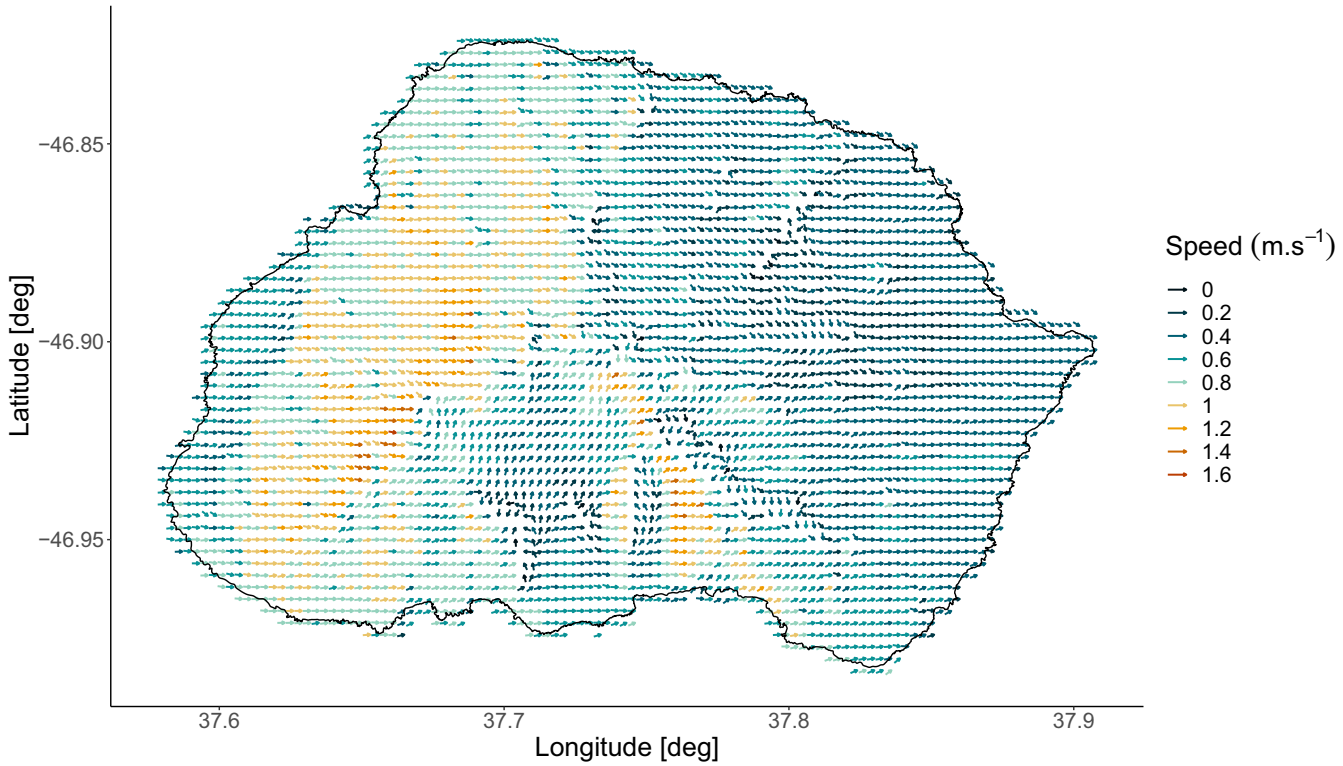

FIGURE 10 | Fine-scale wind vectors (coarsened for visualisation purposes) for a weighted average of the 16 wind direction simulations. Arrows are coloured by vector magnitude (speed).

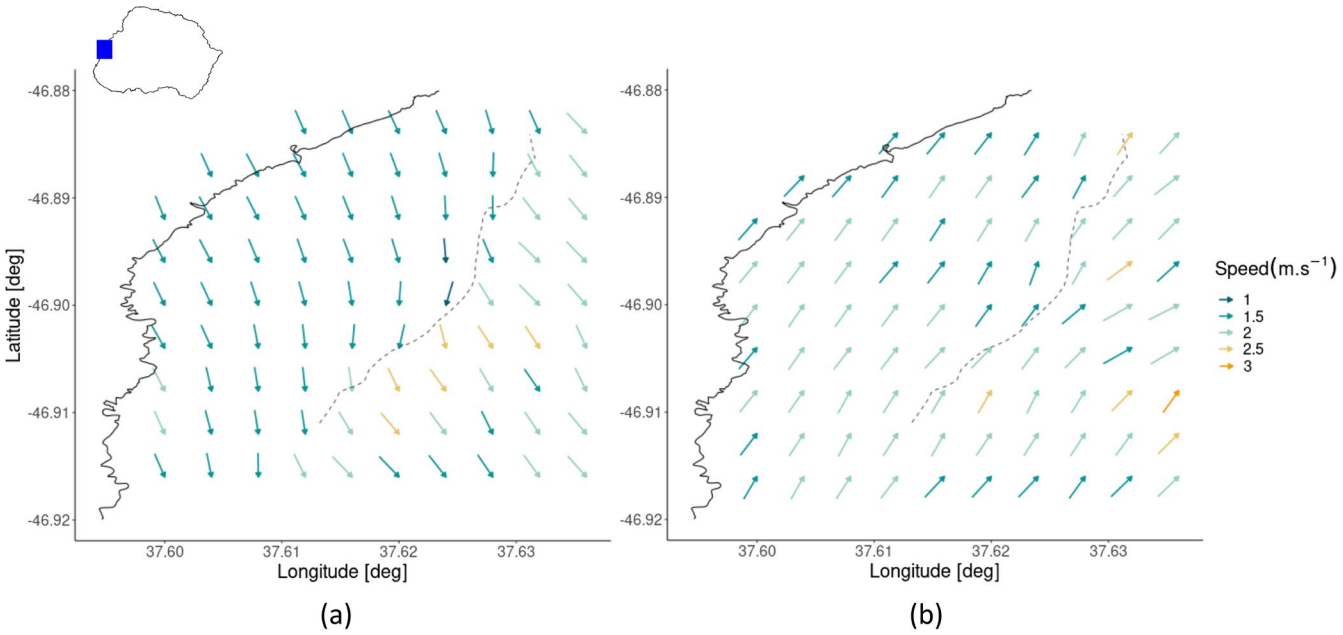

FIGURE 11 | Wind vectors at 1 m a.g.l. from CFD simulations enlarged around the western escarpment for (a) NW and (b) SW inlet conditions. Insert shows the enlarged area and the base of the escarpment is indicated by the dashed grey lines.

The measured data from the 17 locations comprise three comma-separated value (CSV) files: one each for daily, hourly and 10-min data tables, incorporating records from all stations up to 31 May 2021. Only the cleaned data (as discussed above) are included. The coordinates and elevation of each location are given in Table 1 and descriptions of data records for these files are provided in Table 4. The local time on Marion Island is GMT + 3, and all dates and times are reported accordingly. These data are available in Schoombie and le Roux (2025).

The fine-scale wind vectors extracted from the CFD simulations are presented in 16 files (CSV format), each corresponding to a specific freestream wind direction at the domain inlet. All simulations have the same speed condition (see Section 2.3.2).

TABLE 4 | Column headings, their meaning and units for all measured wind data files.

Column heading	Description	Units
Time	Date and time (GMT + 3) in yyyy-mm-dd hh:mm:ss	
StationName	Each station is numbered from 1 to 17. This column provides the name/number of the station where specific data was recorded	
LoggerBatt_Min	Minimum voltage supplied to logger for the sampled period (10 min, hourly or daily)	Volts
LoggerBatt_Max	Maximum voltage supplied to logger for the sampled period (10 min, hourly or daily)	Volts
LoggerBatt_Avg	Average voltage supplied to logger for the sampled period (10 min, hourly or daily)	Volts
LoggerTemp_Min	Minimum logger temperature for the sampled period (10 min, hourly or daily)	°C
LoggerTemp_Max	Maximum logger temperature for the sampled period (10 min, hourly or daily)	°C
LoggerTemp_Avg	Average logger temperature for the sampled period (10 min, hourly or daily)	°C
U_min_1m	Minimum wind speed measured at 1 m for the sampled period (10 min, hourly or daily)	$m \cdot s^{-1}$
U_max_1m	Maximum wind speed measured at 1 m for the sampled period (10 min, hourly or daily)	$m \cdot s^{-1}$
U_sd_1m	Standard deviation of wind speed measured at 1 m for the sampled period (10 min, hourly or daily)	$m \cdot s^{-1}$
U_mean_1m	Average wind speed measured at 1 m for the sampled period (10 min, hourly or daily)	$m \cdot s^{-1}$
Dir_mean_1m	Average wind direction (Campbell Scientific Inc.) measured at 1 m for the sampled period (10 min, hourly or daily). A direction of 0° or 360° corresponds to a N wind, 90° an E wind, 180° a S wind and 270° a W wind.	degrees
Dir_sd_1m	Standard deviation of wind direction measured at 1 m for the sampled period (10 min, hourly or daily)	degrees
U_min_0.5 m	Minimum wind speed measured at 0.5 m for the sampled period (10 min, hourly or daily)	$m \cdot s^{-1}$
U_max_0.5 m	Maximum wind speed measured at 0.5 m for the sampled period (10 min, hourly or daily)	$m \cdot s^{-1}$
U_sd_0.5 m	Standard deviation of wind speed measured at 0.5 m for the sampled period (10 min, hourly or daily)	$m \cdot s^{-1}$
U_mean_0.5 m	Average wind speed measured at 0.5 m for the sampled period (10 min, hourly or daily)	$m \cdot s^{-1}$
Dir_mean_0.5 m	Average wind direction measured at 0.5 m for the sampled period (10 min, hourly or daily). See notes for 'Dir_mean_1m')	degrees
Dir_sd_0.5 m	Standard deviation of wind direction measured at 0.5 m for the sampled period (10 min, hourly or daily)	degrees

The files are named according to the following convention: 'Direction abbreviation'_CFD layers.csv (e.g., 'NNW_CFD-layers.csv' is the file for a north-northwest freestream inlet condition).

The descriptions of the data records for the CFD files are summarised in Table 5. Due to the fine grid spacing (30 × 30 m for an island surface of 17 × 22 km) and because multiple heights a.g.l. are included (see Table 5), the data files are substantial in size (ca. 3.4 GB). These data are available in Schoombie et al. (2025).

4 | Data Usage

A key limitation of the current meteorological monitoring system on Marion Island is that the only full weather station with a sufficiently exposed mast (10 m above ground level, as per World Meteorological Organization guidelines; World Meteorological Organization 2008) is located on the eastern, or lee, side of the island. This study revealed substantial directional variability in wind patterns across Marion Island. Although measurements were conducted at 0.5 and 1 m above ground level, the findings suggest that a weather mast on the windward side of the island would be necessary for more accurate monitoring. However, while the western sector was expected to predominantly reflect the prevailing west to northwesterly winds, this was not observed due to the influence of the western escarpment. This indicates that while establishing a weather mast on the windward side is crucial, its placement requires careful consideration to ensure representative data collection. The combined measured and simulated data from this study provide valuable insights to inform the location of an additional full weather station on the windward side of the island.

The measured and simulated wind data, available at ecologically and geomorphologically relevant heights above ground, can be

TABLE 5 | Meaning of column headings and their units for simulated wind data files.

Column heading	Description	Units
Latitude	Latitudinal coordinate (WGS84) ranging from −46.98317 to −46.82297 (i.e., 46.98317° S to 46.82297° S)	degrees
Longitude	Longitude coordinate (WGS84) ranging from 37.57965 to 37.90811	degrees
Altitude	Height above sea level	m
x.coordinate	Island surface position along the x-axis in the simulation domain, with the origin located offshore to the northeast	m
y.coordinate	Island surface position along the y-axis in the simulation domain, with the origin located offshore to the northeast	m
z.coordinate.AGL	Height above ground level at 0.2, 0.3, 0.5, 1.0, 2.0, 3.0, 4.0, 5.0, 6.0, 7.0, 8.0, 9.0, 10.0, 15.0, 20.0, 25.0, 30.0, 35.0, 40.0, 45.0, 50.0, 55.0, 60.0, 70.0, 80.0, 90.0, 100.0, 120.0, 140.0, 160.0, 180.0 and 200.0	m
x.velocity	Component of the velocity in the x direction (i.e., a positive value means wind blowing from West to East) Commonly used symbol – u	$m \cdot s^{-1}$
y.velocity	Component of the velocity in the y direction (i.e., N-S). A positive value means wind component flowing from South to North Commonly used symbol – v	$m \cdot s^{-1}$
z.velocity	Component of the velocity in the z direction, w (i.e., up or down) Commonly used symbol – w	$m \cdot s^{-1}$
velocity.mag	Three-dimensional velocity magnitude (or 3D speed); Commonly used symbol – U $\lvert U\rvert = \sqrt{u^2 + v^2 + w^2}$	$m \cdot s^{-1}$
turb.intensity	Turbulence intensity (non-dimensional) Commonly used symbol – TI	—
turb.kinetic.energy	Turbulent kinetic energy (see Goddard et al. 2022) Commonly used symbol – k	$m^2 \cdot s^{-2}$
turb.diss.rate	Turbulent kinetic energy dissipation rate (see Goddard et al. 2022) Commonly used symbol – ϵ	$m^2 \cdot s^{-3}$
total.pressure	Total pressure Commonly used symbol – P	Pa
direction.2D	Two-dimensional, horizontal wind direction	degrees

utilised for both island-wide and landform-scale investigations. For example, high-resolution wind vectors can be used to assess their influence on plant growth patterns and functional traits. These datasets can also be used to investigate seabird nesting patterns and quantitatively assess the potential impact of shifts in dominant wind patterns on the breeding conditions of seabirds on Marion Island. Given that several of these species are endangered or threatened, understanding how wind conditions influence their ability to access nesting sites and provide shelter for their chicks is essential for continued conservation efforts (see, e.g., Momberg et al. 2023; Schoombie et al. 2023).

From the dataset of measured wind conditions, we observed that the frequency of calm and windy days varies spatially across Marion Island, but this can be expanded to investigate seasonal differences. The magnitude, timing, and frequency of calm and gale conditions can also be investigated quantitatively from the 10-min, hourly or daily averaged measurements. The upper reaches of the Santa Rosa Valley in Marion Island's southern sector (Figure 1) contain the island's largest and most prominent aeolian features, including mega-ripples, lag gravels, and deflation hollows. This sector of the island experiences more frequent and intense wind events, likely shaping its distinctive aeolian landscape (Nguna 2019). Aeolian transport is driven by gale-force winds due to the power relationship between sediment flux and wind speed (Bagnold 1941). The measured and CFD-derived wind vectors from this study provide high-resolution data to investigate these processes in greater detail, offering new insights into wind-driven sediment transport at both island-wide and landform scales. Additionally, the CFD model can be expanded to simulate other particle flows across the island, such as seed dispersal or the transport of salt spray or ash (the latter in the event of a volcanic eruption).

We have demonstrated how measured and simulated wind datasets can be combined to produce a fine-scale, weighted-average representation of wind vectors at the intra-island scale. This weighted average approach can be modified for specific periods

or geographical sectors, for more targeted quantitative investigations. Additionally, the spatial variability of wind conditions within different altitudinal bands presents an opportunity to investigate whether sheltered high-altitude sites experience lower wind intensities than wind-exposed low-altitude areas.

Although the datasets presented in this study are specific to Marion Island, the methodologies are broadly applicable to other islands. By integrating fine-scale wind modelling with ecological and geomorphological studies, researchers can better assess the role of wind in shaping these ecosystems. Understanding these dynamics is particularly relevant for predicting the impacts of shifting wind patterns in the SO due to climate change.

5 | Conclusions

The presented datasets provide both measured wind data at ecologically relevant heights across multiple locations on Marion Island and high-resolution simulated wind vectors at various altitudes. The combination of measured and modelled data offers a robust foundation for studying the effects of wind on the island's terrestrial ecosystem in conjunction with other biotic and abiotic factors. The simulations allow for an assessment of how wind interacts with the topography of the island under 16 different offshore wind directions, providing insights into potential changes in wind patterns under future climate scenarios. Notably, the measured data reveal a distinct difference in wind conditions at 1 m above ground level between the windward (western) and leeward (eastern) sides of the island, where the SAWS mast is located. This discrepancy indicates the need for a complete weather station on the western side of the island to better capture wind conditions in this exposed region. These data are essential for future research on climate change impacts on terrestrial systems and processes in the sub-Antarctic.

Acknowledgements

The South African Weather Services are acknowledged for providing data from the research station on Marion Island. This study was funded through the South African National Research Foundation under the South African National Antarctic Programme, awarded to Prof. Peter C. le Roux (grant number 110726). This research was conducted under permit (1/2013) from the Prince Edward Island Management Committee. Thank you very much to all the field assistants who helped instal and maintain the equipment as well as download data. In particular, thanks to the assistance from our colleagues, Mr. Zenande Kabase (University of Fort Hare), Dr. Maëlle Connan (Nelson Mandela University), Dr. Elizabeth Rudolph (University of the Free State), Dr. Anton Wolfaardt (Mouse-Free Marion) and Dr. Susie Cunningham (FitzPatrick Institute of African Ornithology, University of Cape Town) for support throughout various aspects of the project.

Disclosure

Code Availability: All data post-processing was conducted in the R statistical programming language. Custom programs for creating wind roses for visualisations in this publication (Dataset 1) will be made available on request. The R script used to calculate a weighted average computational fluid dynamics layer at 1 m a.g.l. (Dataset 2) is provided in Schoombie et al. (2025).

Conflicts of Interest

The authors declare no conflicts of interest.

Data Availability Statement

The data that support the findings of this study are openly available in the South African Polar Research Infrastructure (SAPRI) Data Centre at http://doi.org/10.15493/SAPRI.07032025 and https://doi.org/10.15493/SAPRI.23012025.

References

Anderson, T. R., and M. I. Lucas. 2009. "Upwelling Ecosystems." In *Ecosystem Ecology*, edited by S. E. Jorgensen, 1st ed., 450–460. Elsevier B.V.

ANSYS Inc. 2025. "ANSYS Fluent: Fluid Simulation Software." https://www.ansys.com/products/fluids/ansys-fluent.

Bagnold, R. A. 1941. *The Physics of Blown Sand and Desert Dunes*. Chapman and Hall.

Born, C., P. C. le Roux, C. Spohr, M. A. McGeoch, and B. Jansen van Vuuren. 2012. "Plant Dispersal in the Sub-Antarctic Inferred From Anisotropic Genetic Structure." *Molecular Ecology* 21: 184–194.

Cabezón, D., J. Sumner, B. Garcia, J. Sanz Rodrigo, and C. Masson. 2011. "RANS Simulations of Wind Flow at the Bolund Experiment." European Wind Energy Conference and Exhibition 2011, EWEC 2011, 141–144.

Campbell Scientific Inc. n.d. "CR300 Instructions: Wind Vector (Calculate Wind Vector)." CR Basic Help. Accessed July 30, 2023. https://help.campbellsci.com/crbasic/cr300/Content/Info/wv_calculations.htm.

Chau, J. H., C. Born, M. A. McGeoch, et al. 2019. "The Influence of Landscape, Climate and History on Spatial Genetic Patterns in Keystone Plants (Azorella) on Sub-Antarctic Islands." *Molecular Ecology* 28, no. 14: 3291–3305. https://doi.org/10.1111/mec.15147.

Chown, S. L., and P. Convey. 2016. "Antarctic Entomology." *Annual Review of Entomology* 61: 119–137. https://doi.org/10.1146/annurev-ento-010715-023537.

Chown, S. L., and P. W. Froneman, eds. 2008. *The Prince Edward Islands: Land-Sea Interactions in a Changing Ecosystem*. African SunMedia.

Chown, S. L., P. C. Le Roux, T. Ramaswiela, J. M. Kalwij, J. D. Shaw, and M. A. McGeoch. 2013. "Climate Change and Elevational Diversity Capacity: Do Weedy Species Take Up the Slack?" *Biology Letters* 9, no. 1: 20120806. https://doi.org/10.1098/rsbl.2012.0806.

Clay, T. A., R. Joo, H. Weimerskirch, et al. 2020. "Sex-Specific Effects of Wind on the Flight Decisions of a Sexually Dimorphic Soaring Bird." *Journal of Animal Ecology* 89, no. 8: 1811–1823. https://doi.org/10.1111/1365-2656.13267.

Combrinck, M. L., T. M. Harms, M. A. McGeoch, J. Schoombie, and P. C. le Roux. 2020. "Wind and Seed: A Conceptual Model of Shape-Formation in the Cushion Plant Azorella Selago." *Plant and Soil* 455, no. 1–2: 339–366. https://doi.org/10.1007/s11104-020-04665-3.

Constable, A. J., J. Melbourne-Thomas, S. P. Corney, et al. 2014. "Climate Change and Southern Ocean Ecosystems I: How Changes in Physical Habitats Directly Affect Marine Biota." *Global Change Biology* 20, no. 10: 3004–3025. https://doi.org/10.1111/gcb.12623.

Copernicus Climate Change Service, Climate Data Store. 2023. *ERA5 Hourly Data On Single Levels From 1940 to Present*. Copernicus Climate Change Service (C3S) Climate Data Store (CDS). https://doi.org/10.24381/cds.adbb2d47.

Crasto, G. 2007. *Numerical Simulations of the Atmospheric Boundary Layer*. Università degli Studi di Cagliari. https://windsim.com/Winds

imarchive/library%20--%20papers-presentations/0702_Giorgio_Crasto.pdf.

Department of Environmental Affairs. (2010). Prince Edward Islands management plan (Version 0.2). Prepared by the DST-NRF Centre of Excellence for Invasion Biology, Stellenbosch University. https://www.dffe.gov.za/sites/default/files/docs/princeedward_islands_managementplan.pdf. [Accessed: 25 July 2025].

Gill Instruments Limited. 2017. "WindSonic Manual." https://gillinstruments.com/wp-content/uploads/2025/01/1405-PS-0019-WindSonic-Manual.pdf.

Goddard, K. A. 2021. *Investigation of Wind Patterns on Marion Island Using Computational Fluid Dynamics and Measured Data*. University of Pretoria. https://repository.up.ac.za/handle/2263/78564.

Goddard, K. A., K. J. Craig, J. Schoombie, and P. C. le Roux. 2022. "Investigation of Ecologically Relevant Wind Patterns on Marion Island Using Computational Fluid Dynamics and Measured Data." *Ecological Modelling* 464: 109827. https://doi.org/10.1016/j.ecolmodel.2021.109827.

González-Solís, J., A. Felicísimo, J. W. Fox, V. Afanasyev, Y. Kolbeinsson, and J. Muñoz. 2009. "Influence of Sea Surface Winds on Shearwater Migration Detours." *Marine Ecology Progress Series* 391: 221–230. https://doi.org/10.3354/meps08128.

Hargreaves, D., T. Porter, and N. Wright. 2006. "Consistent Inlet Boundary Conditions in Computational Fluid Dynamics Modelling of Wind Flow Over Terrain." In Proceeding 7th UK Conference on Wind Engineering, Glasgow, UK, pp. 47–50.

Hedding, D. W., and M. Greve. 2018. "Decreases in Precipitation on Sub-Antarctic Marion Island: Implications for Ecological and Geomorphological Processes." *Weather* 73, no. 6: 203. https://doi.org/10.1002/wea.3245.

Hedding, D. W., W. Nel, and R. L. Anderson. 2015. "Aeolian Processes and Landforms in the Sub-Antarctic: Preliminary Observations From Marion Island." *Polar Research* 34: 26365. https://doi.org/10.3402/polar.v34.26365.

Huntley, B. J. 2016. *Exploring a Sub-Antarctic Wilderness: a Personal Narrative of the First Biological and Geological Expedition to Marion and Prince Edward Islands 1965/1966*. Antarctic Legacy of South Africa.

Launder, B. E., and D. B. Spalding. 1974. "The Numerical Computation of Turbulent Flows." *Computer Methods in Applied Mechanics and Engineering* 3, no. 2: 269–289. https://doi.org/10.1016/0045-7825(74)90029-2.

le Roux, P. C. 2008. "Climate and Climate Change." In *The Prince Edward Islands: Land-Sea Interactions in a Changing Ecosystem*, edited by S. L. Chown and P. W. Froneman, 39–64. Stellenbosch University Press. https://doi.org/10.18820/9781928314219/03.

le Roux, P. C., and M. A. McGeoch. 2008a. "Rapid Range Expansion and Community Reorganization in Response to Warming." *Global Change Biology* 14, no. 12: 2950–2962. https://doi.org/10.1111/j.1365-2486.2008.01687.x.

le Roux, P. C., and M. A. McGeoch. 2008b. "Spatial Variation in Plant Interactions Across a Severity Gradient in the Sub-Antarctic." *Oecologia* 155, no. 4: 831–844. https://doi.org/10.1007/s00442-007-0954-1.

Lin, X., X. Zhai, Z. Wang, and D. R. Munday. 2018. "Mean, Variability, and Trend of Southern Ocean Wind Stress: Role of Wind Fluctuations." *Journal of Climate* 31, no. 9: 3557–3573. https://doi.org/10.1175/JCLI-D-17-0481.1.

Manwell, J. F., J. G. McGowan, and A. L. Rogers. 2009. *Wind Energy Explained: Theory, Design and Application*. 2nd ed. John Wiley & Sons, Ltd.

Mazibuko, N., M. Greve, and P. C. le Roux. 2024. "Dispersal Potential Does Not Predict Recent Range Expansions of Sub-Antarctic Plant Species." *Polar Biology* 47, no. 5: 499–514. https://doi.org/10.1007/s00300-024-03250-z.

Mingione, M., F. Lagona, P. Nagar, et al. 2025. "Does Wind Affect the Orientation of Vegetation Stripes? A Copula-Based Mixture Model for Axial and Circular Data." *Environmetrics* 36, no. 5: e70021. https://doi.org/10.1002/env.70021.

Momberg, M., D. W. Hedding, M. Luoto, and P. C. le Roux. 2021a. "Exposing Wind Stress as a Driver of Fine-Scale Variation in Plant Communities." *Journal of Ecology* 109, no. 5: 2121–2136. https://doi.org/10.1111/1365-2745.13625.

Momberg, M., D. W. Hedding, M. Luoto, and P. C. le Roux. 2021b. "Species Differ in Their Responses to Wind: The Underexplored Link Between Species Fine-Scale Occurrences and Variation in Wind Stress." *Journal of Vegetation Science* 32, no. 6: e13093. https://doi.org/10.1111/jvs.13093.

Momberg, M., P. G. Ryan, D. W. Hedding, et al. 2023. "Factors Determining Nest-Site Selection of Surface-Nesting Seabirds: A Case Study on the World's Largest Pelagic Bird, the Wandering Albatross (*Diomedea exulans*)." *Ibis* 165, no. 1: 190–203. https://doi.org/10.1111/ibi.13111.

National Centers for Environmental Information. n.d. "Sea Surface Wind, NOAA NCEI blended daily averaged 0.25° Version 2.0, Science Quality (1987-recent), Daily [Dataset]." NOAA National Centers for Environmental Information. Retrieved from January 20, 2025. https://coastwatch.noaa.gov/erddap/griddap/noaacwBlendedWindsDaily.htmlTable?u_wind%5B(2024-11-30T18:00:00Z)%5D%5B(10.0)%5D%5B(-48.5):(-45.5)%5D%5B(36.0):(39.0)%5D,v_wind%5B(2024-11-30T18:00:00Z)%5D%5B(10.0)%5D%5B(-48.5):(-45.5)%5D%5B(36.0):(39.0)%5D&.dra.

Nel, W., D. W. Hedding, and E. M. Rudolph. 2023. "The Sub-Antarctic Islands Are Increasingly Warming in the 21st Century." *Antarctic Science* 35, no. 2: 124–126. https://doi.org/10.1017/S0954102023000056.

Nguna, A. A. 2019. "Aeolian Processes and Landforms at Mesrug on Sub-Antarctic Marion Island." University of Fort Hare. http://hdl.handle.net/10353/17095.

Perren, B. B., D. A. Hodgson, S. J. Roberts, L. Sime, E. Verleyen, and W. Vyverman. 2020. "Southward Migration of the Southern Hemisphere Over Centennial Timescales." *Communications Earth & Environment* 1: 58. https://doi.org/10.1038/s43247-020-00059-6.

Richardson, P. L., E. D. Wakefield, and R. A. Phillips. 2018. "Flight Speed and Performance of the Wandering Albatross With Respect to Wind." *Movement Ecology* 6: 3. https://doi.org/10.1186/s40462-018-0121-9.

Rouault, M., J. Me, C. J. C. Reason, and J. R. E. Lutjeharms. 2005. "Climate Variability at Marion Island, Southern Ocean, Since 1960." *Journal of Geophysical Research* 110: C05007. https://doi.org/10.1029/2004JC002492.

Rudolph, E. M., D. W. Hedding, P. J. N. De Bruyn, and W. Nel. 2022. "An Open Access Geospatial Database for the Sub-Antarctic Prince Edward Islands." *South African Journal of Science* 118, no. 9/10: 12302. https://doi.org/10.17159/sajs.2022/12302.

Schoombie, J., K. J. Craig, K. A. Goddard, and P. C. le Roux. 2025. *Simulated Wind Vectors Across Marion Island for 16 Different Oncoming Wind Directions*. University of Pretoria. https://doi.org/10.15493/SAPRI.07032025.

Schoombie, J., and P. C. le Roux. 2025. *High-Resolution Wind Speed and Direction Data Collected on Marion Island*. University of Pretoria. https://doi.org/10.15493/SAPRI.23012025.

Schoombie, J., S. Schoombie, M. Connan, et al. 2023. "Impact of Wind on Crash-Landing Mortality in Grey-Headed Albatrosses *Thalassarche chrysostoma* Breeding on Marion Island." *Marine Ecology Progress Series* 723: 213–225. https://doi.org/10.3354/meps14292.

Smith, V. R., and L. Mucina. 2006. "Vegetation of Marion and Prince Edward Islands." In *Vegetation of South Africa, Lesotho and Swaziland*, edited by L. Mucina and M. C. Rutherford, 698–723. South African National Biodiversity Institute.

Swart, N. C., and J. C. Fyfe. 2012. "Observed and Simulated Changes in the Southern Hemisphere Surface Westerly Wind-Stress." *Geophysical Research Letters* 39, no. 16: 6–11. https://doi.org/10.1029/2012GL052810.

Talley, L. D. 2013. "Closure of the Global Overturning Circulation Through the Indian, Pacific, and Southern Oceans: Schematics and Transport." *Oceanography* 26, no. 1: 80–97. https://doi.org/10.5670/oceanog.2013.07.

Thorne, L. H., T. A. Clay, R. A. Phillips, L. G. Silvers, and E. D. Wakefield. 2023. "Effects of Wind on the Movement, Behavior, Energetics, and Life History of Seabirds." *Marine Ecology Progress Series* 723: 73–117. https://doi.org/10.3354/meps14417.

Toolsee, T., and T. Lamont. 2022. "Long-Term Trends and Interannual Variability of Wind Forcing, Surface Circulation, and Temperature Around the Sub-Antarctic Prince Edward Islands." *Remote Sensing* 14, no. 6: 1318. https://doi.org/10.3390/rs14061318.

Weimerskirch, H., M. Louzao, S. De Grissac, and K. Delord. 2012. "Changes in Wind Pattern Alter Albatross Distribution and Life-History Traits." *Science* 335, no. 6065: 211–214. https://doi.org/10.1126/science.1210270.

World Meteorological Organization. 2008. "Measurement of Surface Wind." In *Guide to Meteorological Instruments and Methods of Observation*, 7th ed. World Meteorological Organization.

Supporting Information

Additional supporting information can be found online in the Supporting Information section. **Data S1:** gdj370035-sup-0001-Figures.docx.